International Journal of
Science, Architecture, Technology and Environment

Analysis of MHD Heat and Mass Transfer in a Microchannel with Viscous Dissipation and Linear Thermal Radiation Effects

Sanni Saudat[1*], Hussaini Abdullahi[2]

[1]*Department of Mathematics, Federal College of Education, Gidan Madi, Tangaza, Sokoto State, Nigeria*

[2]*Department of Mathematics, Sokoto State University, Sokoto, Nigeria*

[*]*Corresponding author*

DOI: https://doi.org/10.63680/ijsate062614.18

Abstract

This study examines magnetohydrodynamic (MHD) heat and mass transfer in a microchannel with viscous dissipation and linear thermal radiation effects. The governing nonlinear equations are nondimensionalized and solved numerically using an implicit finite difference scheme, while an analytical perturbation method is employed to validate the numerical results. The influence of key parameters on velocity, temperature, and concentration profiles is analyzed. Results indicate that buoyancy enhances fluid velocity, while magnetic effects suppress the flow. An increase in the Prandtl number reduces the thermal boundary layer thickness and enhances heat transfer, whereas viscous dissipation and thermal radiation elevate the fluid temperature. Increasing Schmidt number and chemical reaction parameter decrease concentration profiles. Skin friction rises with buoyancy but decreases with Casson and magnetic parameters. Heat transfer improves with Prandtl number but reduces with radiation, while mass transfer increases with Schmidt number and chemical reaction. These results are relevant to engineering applications involving non-Newtonian fluid flow.

Keywords: Casson fluid, Magnetohydrodynamic (MHD), Natural convection, thermal radiation, chemical reaction

Nomenclature

g	acceleration due to gravity
T'	fluid temperature
T_∞	ambient/free-stream temperature
C'	species concentration in the fluid
B_0	applied magnetic field strength
u'	fluid velocity in the flow direction
t'	dimensional time
y'	spatial coordinate normal to the plate
C_∞	ambient/free-stream concentration
k_0	permeability of the porous medium
C_p	specific heat capacity at constant pressure
K	thermal conductivity of the fluid
q_r	radiative heat flux
R_p	chemical reaction rate parameter
D_0	mass diffusivity
Ca	Casson parameter (dimensionless)
Gr	thermal Grashof number
Gc	solutal Grashof
R_c	chemical reaction parameter
Pr	Prandtl number
u	dimensionless fluid velocity in x direction
t	dimensionless time
C	dimensionless species concentration
F	porosity parameter
F_m	magnetic parameter
Sc	Schmidt number
Rd	Radiation parameter
Ec	Eckert number

Greek symbols

γ	Casson Parameter
ρ	fluid density
θ	dimensionless fluid temperature
μ	dynamic viscosity of the fluid
σ	electrical conductivity of the fluid
α	weighing factor/parameter ($\alpha = 1$)
ψ	represent u, θ, c respectively
β_T	thermal expansion coefficient
β_C	solutal concentration expansion coefficient
μ_B	plastic dynamic viscosity (Casson fluid viscosity coefficient)
ϕ	porosity of the porous medium
υ	kinematic viscosity coefficient

1 Introduction

Heat and mass transfer in fluid flow over vertical surfaces has attracted considerable attention because of its wide range of applications in engineering and industrial processes, including heat exchangers, cooling systems, geothermal energy extraction, filtration systems, chemical reactors, and energy conversion devices. The increasing demand for efficient energy utilization and improved thermal performance has motivated extensive studies on boundary layer transport phenomena. Recent investigations have shown that the combined effects of heat and mass transfer significantly influence flow stability and thermal efficiency in engineering systems (Lund et al. [1]; Anwar et al. [2]).

Among the various factors influencing transport phenomena, magnetohydrodynamic (MHD) effects play a significant role in systems involving electrically conducting fluids such as metallurgical processes, cooling of nuclear reactors, magnetic drug targeting, and electromagnetic flow control. The application of a magnetic field introduces a Lorentz force

that opposes fluid motion, thereby modifying velocity, temperature, and concentration distributions within the boundary layer. Rasheed et al. [3] examined unsteady MHD Casson fluid flow and found that increasing the magnetic parameter suppresses velocity due to resistive forces. Similarly, Hassan et al. [4]; Chamkha and Rashad [5] reported that increasing the magnetic parameter leads to a reduction in fluid velocity while enhancing thermal characteristics due to resistive heating effects. Furthermore, studies by Abdullahi and Yabo [6] & [7] on MHD free convection in porous media have shown that magnetic fields suppress fluid motion whereas buoyancy enhances flow. Shah et al. [8] extended these studies to unsteady conditions and demonstrated that time-dependent MHD Casson fluid flow with chemical reaction significantly alters both thermal and concentration boundary layers. These findings demonstrate the importance of incorporating magnetic and non-Newtonian effects in realistic transport models.

In many practical applications, fluid flow also occurs through porous media, such as packed-bed reactors, geothermal reservoirs, catalytic reactors and filtration systems. The presence of porous resistance introduces drag forces that influence fluid transport characteristics. Das et al. [9] demonstrated that the interaction between porous resistance and buoyancy forces results in complex flow structures that require detailed mathematical modelling. Additionally, viscous dissipation is another important mechanism in high-speed flows or flows with large velocity gradients, where mechanical energy is converted into thermal energy. This effect, characterized by the Eckert number, leads to an increase in fluid temperature and becomes particularly significant in fluids with high viscosity or low thermal diffusivity. Mabood et al. [10] reported that viscous dissipation enhances thermal boundary layer thickness and enhances heat transfer rates in boundary layer flows. Thermal radiation also plays a dominant role in high-temperature environments such as gas turbines, nuclear reactors, solar collectors, and thermal insulation systems where radiative heat transfer significantly alters thermal boundary layer behaviour (Hassan et al. [4]).

Mass transfer accompanied by chemical reaction is commonly encountered in combustion processes, catalytic reactors, drying technologies, and environmental systems. The Schmidt number governs species diffusion, while the chemical reaction parameter determines the rate of species consumption or generation. Ali et al. [11] reported that the combined influence of diffusion and reaction significantly alters concentration distribution and mass transfer rates.

Despite extensive studies on Casson fluid flow under MHD conditions, previous research has mostly considered isolated or partially coupled physical effects. Limited attention has been

given to the simultaneous interaction of magnetic field, porous medium resistance, viscous dissipation, thermal radiation, and chemical reaction in unsteady natural convection flow over a vertical plate. This coupling leads to a highly nonlinear system of governing equations, rendering analytical solutions challenging and necessitating numerical techniques.

Motivated by these gaps, the present study investigates steady and unsteady natural convection flow of a Casson fluid over a vertical plate by incorporating magnetohydrodynamics effects, drag force resistance, viscous dissipation, thermal radiation, and chemical reaction. Numerical solutions are obtained and validated using analytical approximations to provide a more realistic representation of multiphysics transport phenomena.

2 Problem Formulation

Consider the region above an accelerated plate with an assumed porous medium and the MHD Casson fluid model's incompressible transient flow. A homogenous transverse magnetic field B_0 is applied in a perpendicular line to the y-axis. The Casson fluid's initial flow velocity profile is zero at time t = 0. The velocity is applied perpendicular to a constant magnetic field of intensity B_0. When compared to the applied magnetic field, the generated magnetic field is insignificant.

Under specific assumptions, the following equations constitute the governing equations for the MHD boundary layer flow of Casson fluid:

Momentum equation

$$\rho \frac{\partial u'}{\partial t'} = \mu_B \left(1 + \frac{1}{\gamma}\right) \frac{\partial^2 u'}{dy'^2} + \rho g \beta_T (T' - T_\infty) - \frac{\mu \phi}{k_0} u' - \sigma B_0^2 u' + \rho g \beta_C (C' - C_\infty) \quad (1)$$

Heat transfer equation

$$\rho C_p \frac{\partial T'}{\partial t'} = K \frac{\partial^2 T'}{\partial y'^2} - \left(\frac{1}{\rho C_p}\right) \frac{\partial q_r}{\partial y'} + \mu \left(\frac{\partial u'}{\partial y'}\right)^2 \quad (2)$$

Mass transfer equation

$$\frac{\partial C'}{\partial t'} = D_0 \frac{\partial^2 C'}{\partial y'^2} - R_p (C' - C_\infty) \quad (3)$$

The initial and boundary conditions are:

$$\left.\begin{array}{l} u(y,0) = 0, T(y,0) = T_w, C(y,0) = C_w, for\ all\ y \geq 0, \\ u(0,t) = 0, T(0,t) = T_w, C(0,t) = C_w \text{ at } y = 0, \\ C(y,t) \to C_w, u(y,t) = 0, T(y,t) = T_w \text{ as } y = 1 \end{array}\right\} \quad (4)$$

Whereby u^* dimensional velocity, T^*represent dimensional fluid temperature, C^* represent dimensional concentration, t^* represent dimensional time, y^* represent dimensional coordinate normal to the plate/surface, ρ represent fluid density, g represent acceleration due

to gravity, $q_r$represent radiative heat flux, μ_B represent Casson fluid viscosity parameter, γ represent Casson parameter, B_0 represent magnetic field strength, k_0 represent permeability of porous medium, μ_B represent thermal expansion coefficient, T_∞ ambient temperature far from the surface, ϕ represent porosity parameter of the porous medium, μ represent dynamic viscosity of the fluid, σ represent electrical conductivity of the fluid, β_C represent concentration expansion coefficient, C_p specific heat capacity at constant pressure, C_∞ represent dimensional species concentration, K thermal conductivity of the fluid, D_0 represent mass diffusivity (coefficient of the mass diffusion), R_p represent dimensional chemical reaction rate parameter. Here, B_0 represents the uniform magnetic field applied perpendicular to the flow direction, while k_0 denotes the permeability of the porous medium. The parameter γ characterizes the non-Newtonian Casson fluid behavior, and R_p accounts for the first-order homogeneous chemical reaction effect.

According to Rosseland [12] radiative heat transfer in optically thick media can be approximated by a diffusion process in which the radiative heat flux is proportional to the temperature gradient. Consequently, the Rosseland radiation model is incorporated into the energy equation as:

$$q_r = -\frac{4\sigma^*}{3k^*}\frac{\partial T^4}{\partial y} \tag{5}$$

Where:

σ^* = Stefan-Boltzmann constant

k^* = mean absorption coefficient

T^4 = black-body radiation law, which can be expanded as the linear temperature function. Using Taylor series expanding T^4 about T_∞ and neglecting higher order term, we get

$$T^4 \approx 4T_\infty^3 T - 3T_\infty^4 \tag{6}$$

So:

$$\frac{\partial q_r}{\partial y} = -\frac{16\sigma^* T_\infty^3}{3k^*}\frac{\partial^2 T}{\partial y^2} \tag{7}$$

We introduce non-dimensional dependent and independent variables according:

$$\mathrm{C} = \frac{C^* - C_\infty}{C_w - C_\infty},\ \mathrm{T} = \frac{T^* - T_\infty}{T_w - T_\infty},\ \mathrm{u} = \frac{u^*}{u_w},\ \mathrm{t} = \frac{u_w^2 t^*}{\upsilon},\ \mathrm{y} = \frac{u_w y^*}{\upsilon},\ \mathrm{Ca} = \frac{\mu_B}{\rho\upsilon}\left(1 + \frac{1}{\gamma}\right),\ \mathrm{F} = \frac{\upsilon\mu\phi}{\rho u_w^2 k_0},\quad F_m = \frac{\upsilon\sigma B_0^2}{\rho u_w^2},$$

$$\mathrm{Gr} = \frac{g\beta_T(T_w - T_\infty)\upsilon}{u_w^2},\ \mathrm{Gc} = \frac{g\beta_c(C_w - C_\infty),\upsilon}{u_w^2},\ \mathrm{Ec} = \frac{u_w^2}{C_p(T_w - T_\infty)},\ \mathrm{Pr} = \frac{K}{\upsilon\rho C_p},\ \mathrm{Rd} = \frac{4\sigma^* T_\infty^3}{k^* K},\ \mathrm{Sc} = \frac{\upsilon}{D_0},$$

$$R_c = \frac{\upsilon}{u_w^2} R_p \tag{8}$$

Substituting equation (8) into equations (1) – (3) subject to equation (4) gives the following dimensionless equations:

$$\frac{\partial u}{\partial t} = Ca\frac{\partial^2 u}{\partial y^2} - (F + F_m)u + G_r\theta + G_c C \quad (9)$$

$$\frac{\partial \theta}{\partial t} = \left(1 + \frac{4}{3}Rd\right)\frac{1}{Pr}\frac{\partial^2 \theta}{\partial y^2} + Ec\left(\frac{\partial u}{\partial y}\right)^2 \quad (10)$$

$$\frac{\partial C}{\partial t} = \frac{1}{Sc}\frac{\partial^2 C}{\partial y^2} - R_c C \quad (11)$$

The corresponding initial and boundary conditions are:

$$u(y, 0) = 0,\ \theta(y, 0) = 0,\ C(y, 0) = 0,\ 0 \le y \le 1 \quad (12)$$

$$t > 0 \begin{cases} u = 0,\ C = 1, \theta = 1\ at\ y = 0 \\ u = 0, C = 0, \theta = 0\ at\ y = 1 \end{cases} \quad (13)$$

3 Method of Solutions

The dimensionless Equations (9)–(11) were solved using an implicit finite difference scheme, subject to the initial and boundary conditions specified in Equations (12)-(13). All time derivatives were discretized using the backward difference scheme, whereas second-order spatial derivatives were approximated using central difference schemes evaluated at the advanced time level j+1. A weighting parameter α was introduced to generalize the spatial discretization. The second-order spatial derivative is expressed as a weighted combination of values at the current and advanced time levels. When α = 0, the scheme reduces to an explicit method, while α = 1 yields a fully implicit method. The case α = 0.5 corresponds to the Crank–Nicolson scheme, which is second-order accurate in both space and time and unconditionally stable. This study employed α = 1 making the scheme fully implicit and unconditionally stable. Using the finite difference approximation, we obtain the following set of linear algebraic equations as:

$$r_1 U_{i-1}^{j+1} + (1 + 2r_1)U_i^{j+1} - r_1 U_{i+1}^{j+1} = \left(1 - 2r_2 - \Delta t(F + F_M)\right)U_i^j + r_2 U_{i-1}^j + r_2 U_{i+1}^j + \Delta t Gr\theta_i^j + \Delta t Gc C_i^j \quad (14)$$

$$-r_3\theta_{i-1}^{j+1} + (1 + 2r_3)\theta_i^{j+1} - r_3\theta_{i+1}^{j+1} = (1 - 2r_4)\theta_i^j + r_4\theta_{i-1}^j + r_4\theta_{i+1}^j + r_5\left(U_{i+1}^j - U_{i-1}^j\right)^2 \quad (15)$$

$$-r_6 C_{i-1}^{j+1} + (1 + 2r_6)C_i^{j+1} - r_6 C_{i+1}^{j+1} = (1 - 2r_7 - \Delta t R_c)C_i^j + r_7 C_{i-1}^j + + r_7 C_{i+1}^j \quad (16)$$

Where:

$r_1 = \frac{\alpha \Delta t Ca}{(\Delta y)^2}$; $r_2 = \frac{(1-\alpha)\Delta t Ca}{(\Delta y)^2}$; $a_1 = 1 + \frac{4}{3}Rd$; $a_3 = \frac{a_1}{Pr}$; $r_3 = \frac{a_3 \alpha \Delta t}{(\Delta y)^2}$; $r_4 = \frac{a_3(1-\alpha)\Delta t}{(\Delta y)^2}$; $r_5 = \frac{Ec\Delta t}{4(\Delta y)^2}$;

$a_2 = \frac{1}{Sc}$; $r_6 = \frac{a_2 \alpha \Delta t}{(\Delta y)^2}$; $r_7 = \frac{a_2(1-\alpha)\Delta t}{(\Delta y)^2}$

The resulting system of algebraic equations was solved iteratively at each time level. MATLAB was used for the computational implementation.

4 Surface Transport Coefficients

The skin friction coefficient, Nusselt number, and Sherwood number are collectively referred to as surface transport coefficients or boundary-layer surface characteristics, as they describe the rates of momentum, heat, and mass transfer at the wall, respectively. These parameters are important in analyzing the physical behavior of fluid flow over a surface. Since the governing equations are solved numerically, these derivatives are approximated using second-order finite difference schemes.

At the lower wall boundary (y = 0), a second-order accurate forward difference scheme is employed.

Assuming a general linear combination of the form:

$$\psi_0' = A\psi_0 + B\psi_1 + C\psi_2 \quad (17)$$

Where:

ψ = u, C and θ respectively.

Expanding ψ_1 and ψ_2 about y_N using Taylor series and substituting into equation (17), collecting like terms and matching the ψ_N terms, we obtain the coefficients A, B and C.

$$A = -\frac{3}{2dy}, B = \frac{2}{dy} \text{ and } C = -\frac{1}{2dy} \quad (18)$$

Substituting equation (18) into equation (17), we obtain the Skin friction, Nusselt and Sherwood number respectively at the lower wall.

$$SK_0 = \frac{-3u_0 + 4u_1 - u_2}{2\Delta y} \quad (19)$$

$$NU_0 = \frac{-3\theta_0 + 4\theta_1 - \theta_2}{2\Delta y} \quad (20)$$

$$SHE_0 = \frac{-3C_0 + 4C_1 - C_2}{2\Delta y} \quad (21)$$

At the upper wall boundary (y = 1), a second-order accurate backward difference scheme is used. A similar procedure is followed by assuming:

$$\psi_1' = A\psi_N + B\psi_{N-1} + C\psi_{N-2} \quad (22)$$

Expanding ψ_{N-1} and ψ_{N-2} about y_1 using Taylor series and substituting into equation (22). collecting like terms and matching the ψ_0 terms, we obtain the coefficient A, B and C.

$$A = \frac{3}{2dy}, B = -\frac{2}{dy} \text{ and } C = \frac{1}{2dy} \quad (23)$$

Substituting equation (23) into equation (22), we obtain the Skin friction, Nusselt and Sherwood numbers respectively at the upper wall.

$$SK_1 = \frac{3u_0 - 4u_1 + u_2}{2\Delta y} \quad (24)$$

$$NU_1 = \frac{3\theta_0 - 4\theta_1 + \theta_2}{2\Delta y} \quad (25)$$

$$SHE_1 = \frac{3C_0 - 4C_1 + C_2}{2\Delta y} \quad (26)$$

5 Perturbation Technique

The perturbation technique is an analytical method used to obtain approximate solutions to nonlinear differential equations that are difficult to solve exactly. It is widely used in fluid flow, heat transfer, and mass transfer problems due to its simplicity and effectiveness in handling weakly nonlinear systems. The method is based on the introduction of a small parameter into the dimensionless equations, which allows the solution to be expressed as a series expansion in terms of that parameter. In this study, the Prandtl number (Pr) is considered as the perturbation parameter, and the solution is obtained up to the first-order approximation.

To validate the numerical method, an analytical perturbation technique was employed under steady-state conditions. The dependent variables were expanded in perturbation series as:

$$\left.\begin{aligned} u(y) &= u_0(y) + \mathrm{Pr}u_1(y) \\ \theta(y) &= \theta_0(y) + \mathrm{Pr}\theta_1(y) \\ C(y) &= C_0(y) + \mathrm{Pr}C_1(y) \end{aligned}\right\} \quad (27)$$

Substituting the perturbation expansions into the dimensionless equations at steady state and equating coefficients of like powers of the perturbation parameter produced solvable ordinary differential equations.

The analytical solutions obtained were compared with the numerical results to verify the accuracy of the computational method.

6 Results and Discussion

The effects of various governing parameters on velocity, temperature, and concentration profiles were examined.

Results Validation

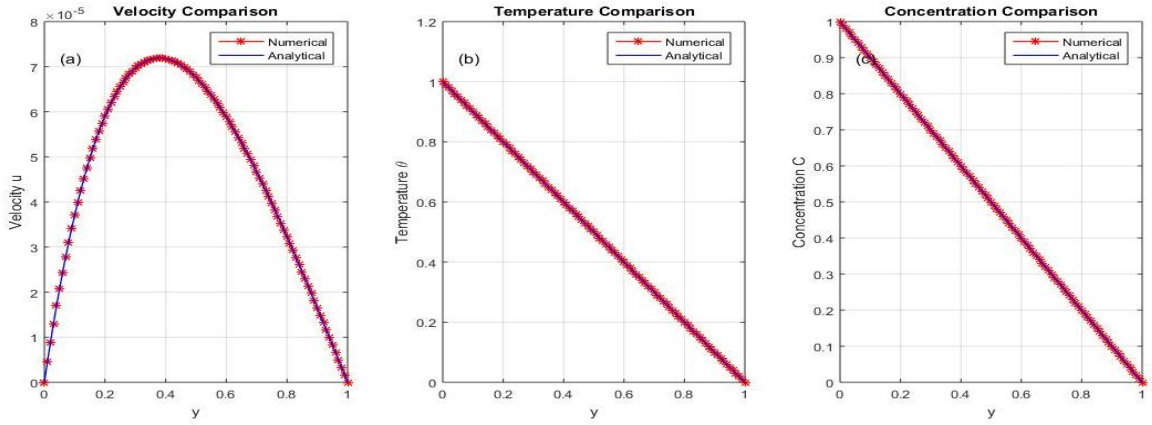

Figure 1: Comparison of numerical and analytical solutions for (a) velocity u, (b) temperature θ, and (c) concentration C profiles.

To ensure the accuracy and reliability of the numerical scheme employed in this study, the results obtained using the finite difference method were validated against the analytical solutions derived using the perturbation technique. Figure 1 shows excellent agreement between the two approaches, with nearly overlapping curves for the velocity, temperature, and concentration profiles throughout the computational domain. The maximum absolute error was found to be negligibly small, confirming the accuracy, convergence, and stability of the numerical method. Hence, the finite difference scheme is reliable for predicting the flow, thermal, and concentration characteristics of the present problem.

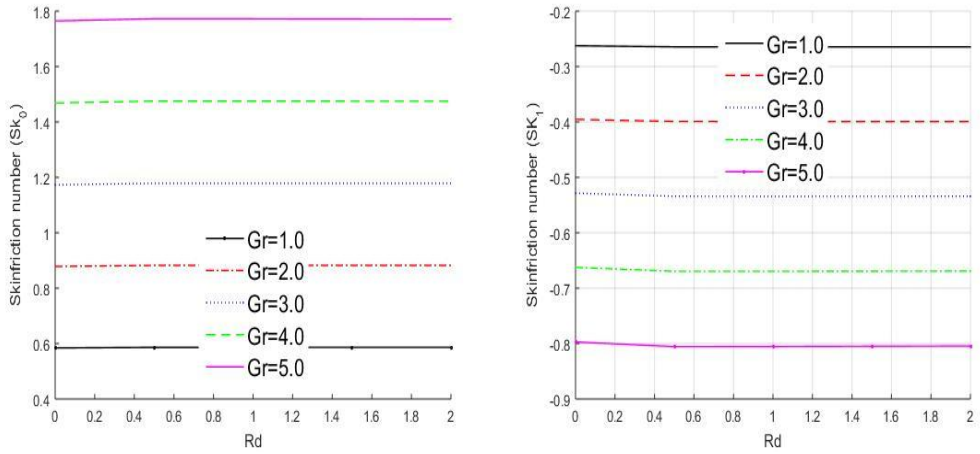

Figure 2: Variation of skin friction coefficient SK with radiation parameter Rd for different values of solutal Grashof number Gr

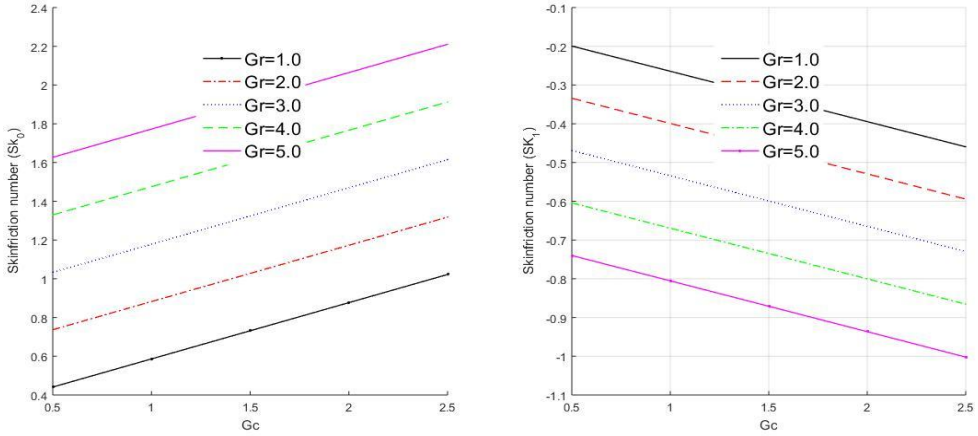

Figure 3: Variation of skin friction coefficient SK with solutal Grashof number Gc for different values of thermal Grashof number Gr.

Figures 2 and 3 illustrate the variation of skin friction with different parameters. Skin friction is only weakly influenced by the radiation parameter R_d (Figure 2), whereas it increases with increasing thermal Grashof number Gr, indicating the dominance of buoyancy forces. Figure 3 shows that increasing solutal Grashof number Gc enhances skin friction due to stronger concentration-driven buoyancy.

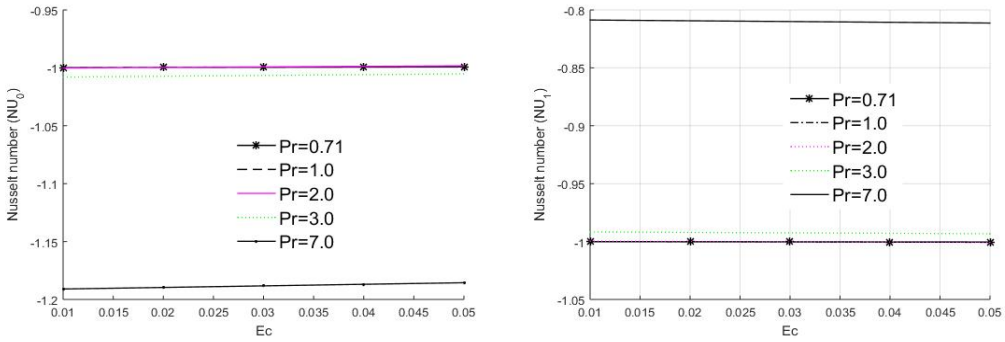

Figure 4: Variation of Nusselt number NU with Eckert number Ec for different values of Prandtl number Pr

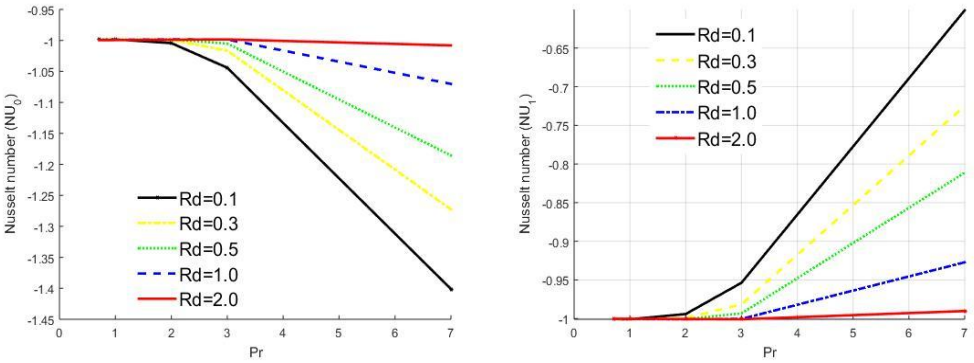

Figure 5: Variation of Nusselt number NU with Prandtl number Pr for different values of Radiation parameter Rd

Figures 4 and 5 present the variation of the Nusselt number. Figure 4 shows the variation of the Nusselt number with Eckert number for different values of the Prandtl number. The Nusselt number is only weakly affected by changes in the Eckert number, as evidenced by the nearly horizontal curves. However, increasing the Prandtl number increases the Nusselt number, indicating enhanced heat transfer at the wall. This enhancement is attributed to the reduction in thermal diffusivity associated with larger Prandtl numbers, which leads to thinner thermal boundary layers and larger temperature gradients at the surface. Consequently, the Prandtl number exerts a much stronger influence on heat transfer than the Eckert number within the present parameter range. Figure 5 shows that the Nusselt number increases with increasing Prandtl number, indicating enhanced heat transfer due to reduced thermal diffusivity and thinner thermal boundary layers. However, increasing the radiation parameter decreases the Nusselt number, demonstrating that thermal radiation suppresses the wall heat transfer rate by reducing the temperature gradient at the surface.

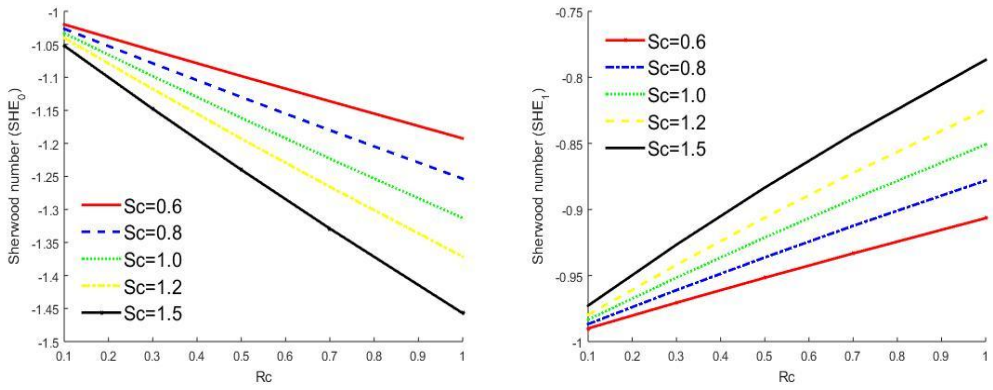

Figure 6: Variation of Sherwood number SHE with chemical reaction R_c parameter for different values of Schmidt number Sc

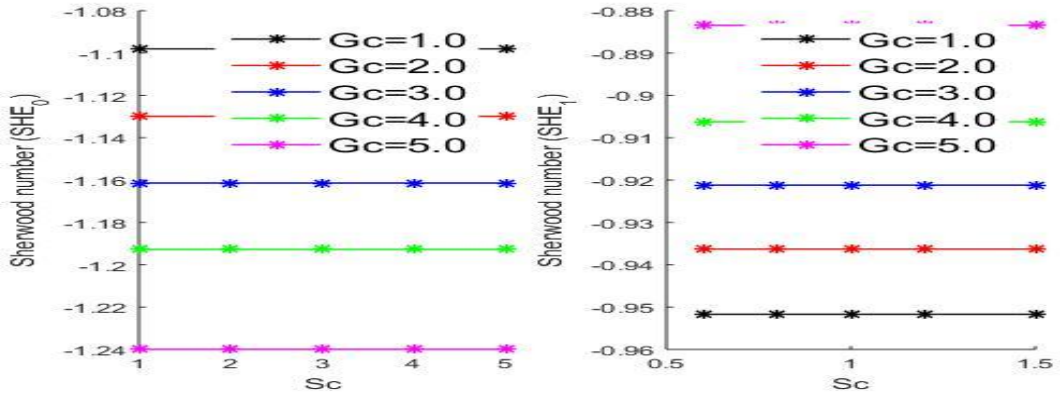

Figure 7: Variation of Sherwood number SHE with solutal Grashof number Gc parameter for different values of Schmidt number Sc

Figure 6 demonstrates that the Sherwood number increases with increasing Schmidt number Sc, which is attributed to lower mass diffusivity and a thinner concentration boundary layer. Figure 7 indicates that variations in the solutal Grashof number Gc have only a marginal influence on the Sherwood number, whereas the Schmidt number remains the dominant parameter governing mass transfer.

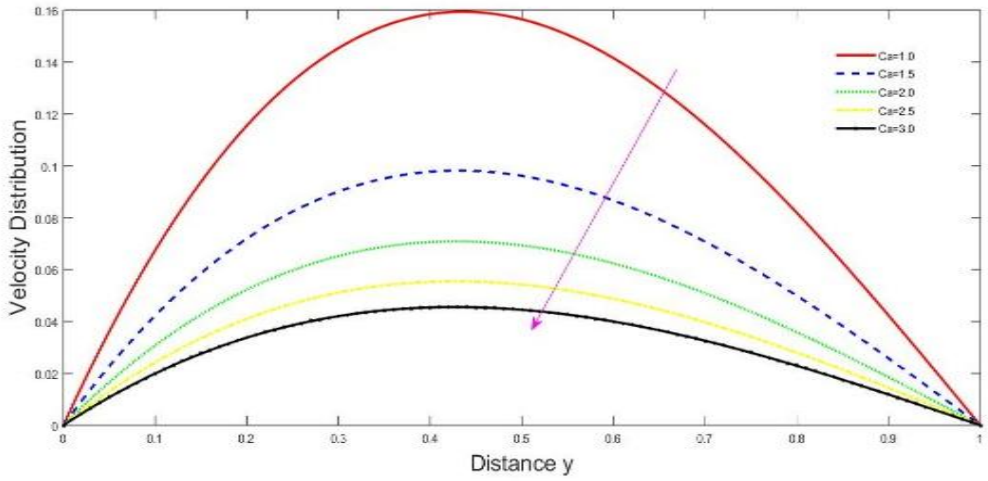

Figure 8: Effect of the Casson parameter Ca on the velocity distribution.

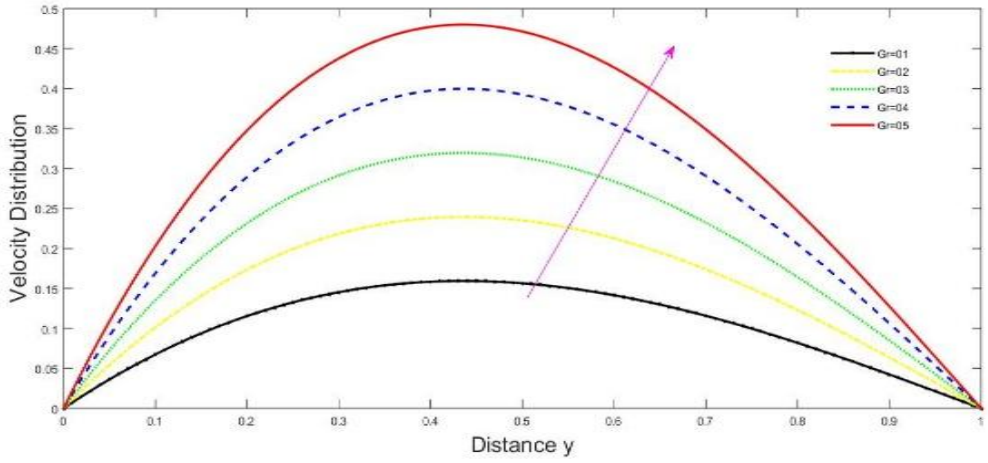

Figure 9: Effect of the thermal Grashof number Gr on the velocity distribution.

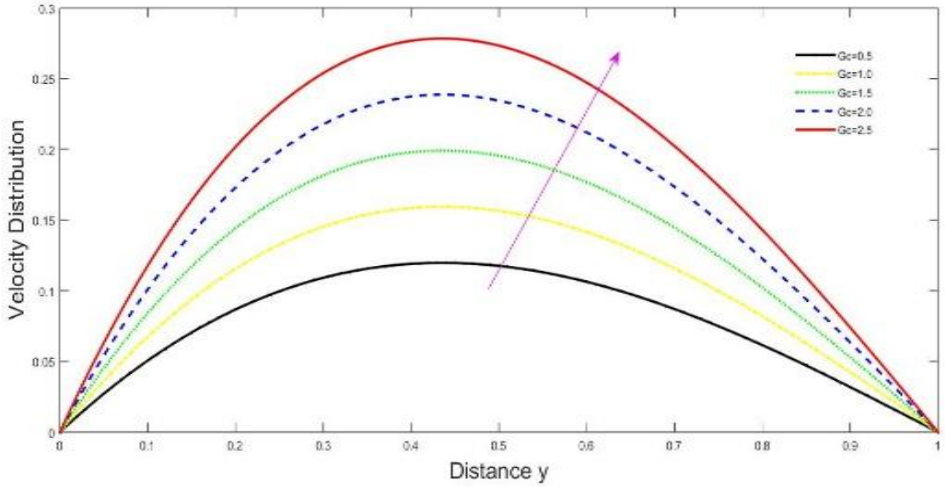

Figure 10: Effect of solutal Grashof number Gc on the velocity distribution

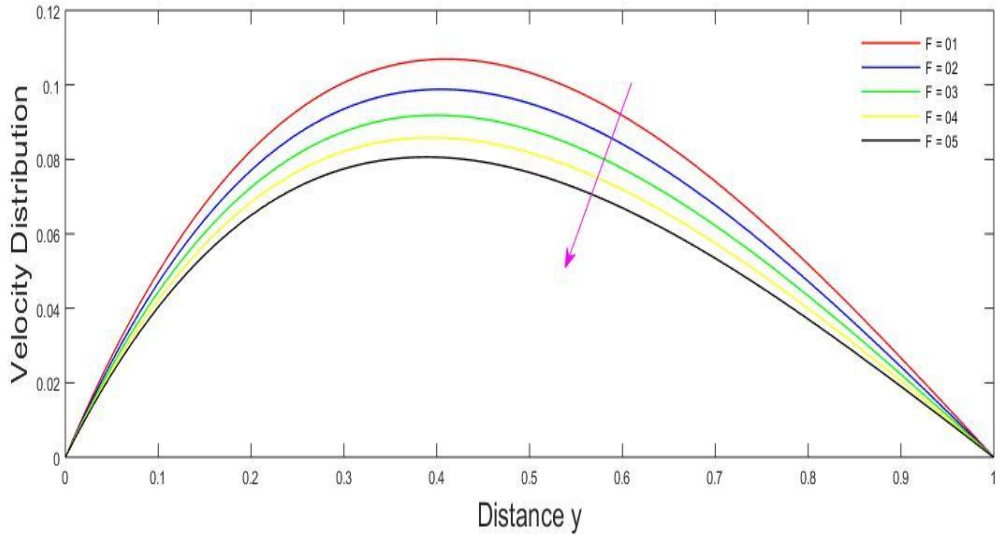

Figure 11: Effect of porosity parameter (F) on Velocity Profile

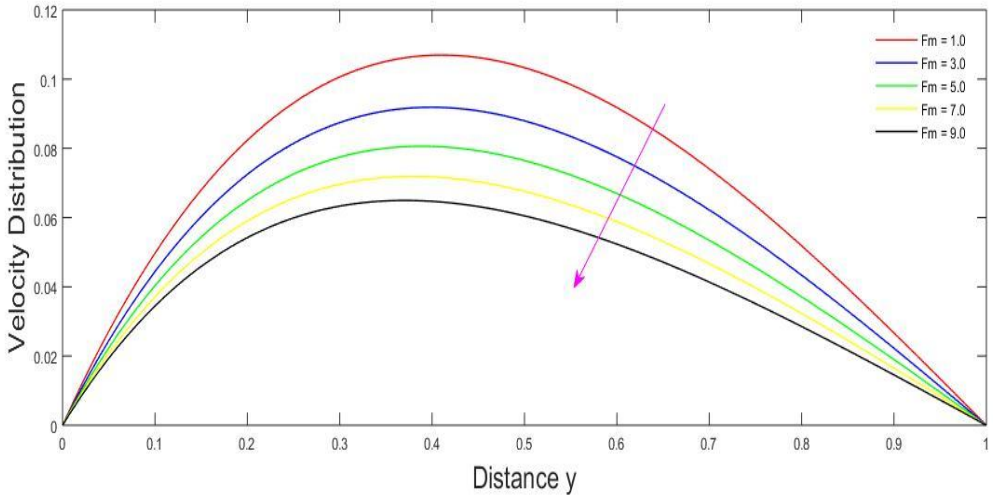

Figure 12: Effect of magnetic parameter (Fm) on Velocity Profile

Figures 8 - 12 illustrate the effects of governing parameters on the velocity profile. Increasing the Casson parameter Ca (Figure 8) reduces velocity due to increased effective viscosity, which resists fluid motion. In contrast, higher thermal and solutal Grashof numbers Gr and Gc (Figures 9 and 10) enhance velocity as a result of stronger buoyancy forces. Similarly, an increase in the porosity parameter F (Figure 11) decreases velocity throughout the flow region. This occurs because higher values of F correspond to stronger porous medium resistance, which opposes the fluid motion. Similarly, as the magnetic parameter Fm increases (Figure 12), the fluid velocity decreases across the boundary layer region. This behavior occurs because a stronger magnetic field generates a larger Lorentz force, which acts opposite to the direction of fluid motion.

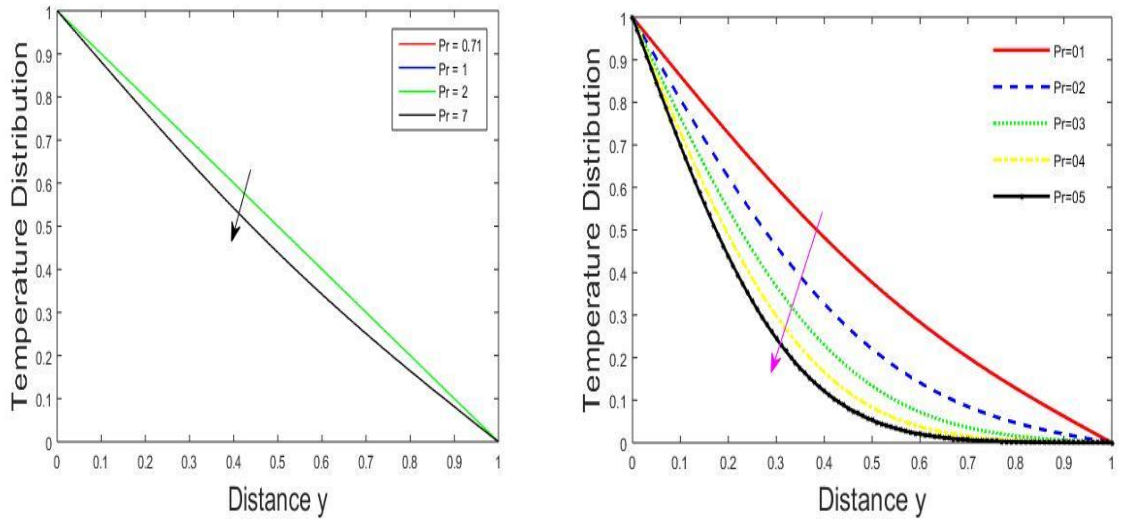

Figure 13: Effect of Prandtl parameter (Pr) on Temperature Profile

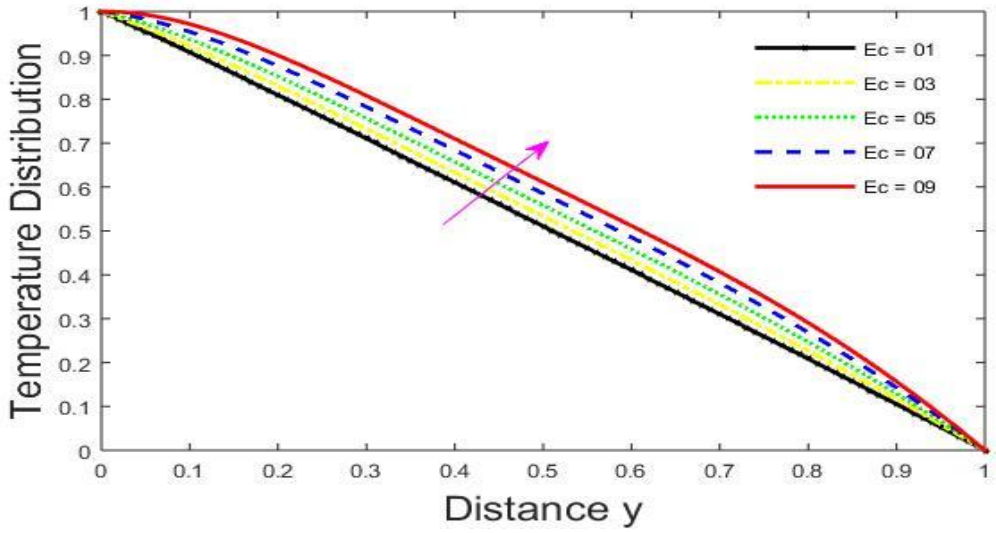

Figure 14: Effect of Eckert parameter (Ec) on Temperature Profile

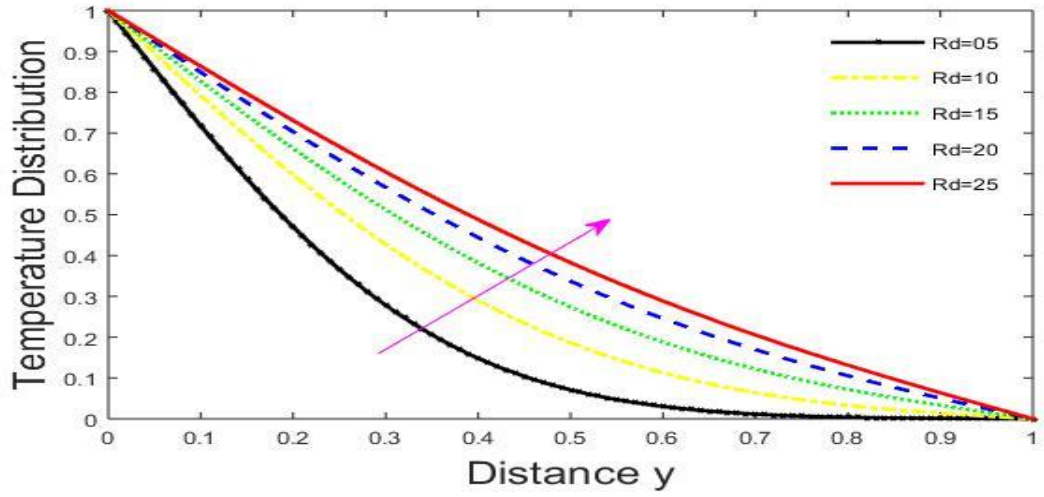

Figure 15: Effect of Radiation parameter (Rd) on Temperature Profile

Figures 13 – 15 present the variation of temperature with different parameters. An increase in the Prandtl number Pr (Figure 13) decreases temperature due to reduced thermal diffusivity, resulting in a thinner thermal boundary layer. Conversely, higher Eckert number Ec (Figure 14) increases temperature due to viscous dissipation, which converts kinetic energy into thermal energy. Similarly, increasing the radiation parameter Rd (Figure 15) raises the temperature as a result of enhanced radiative heat transfer within the fluid.

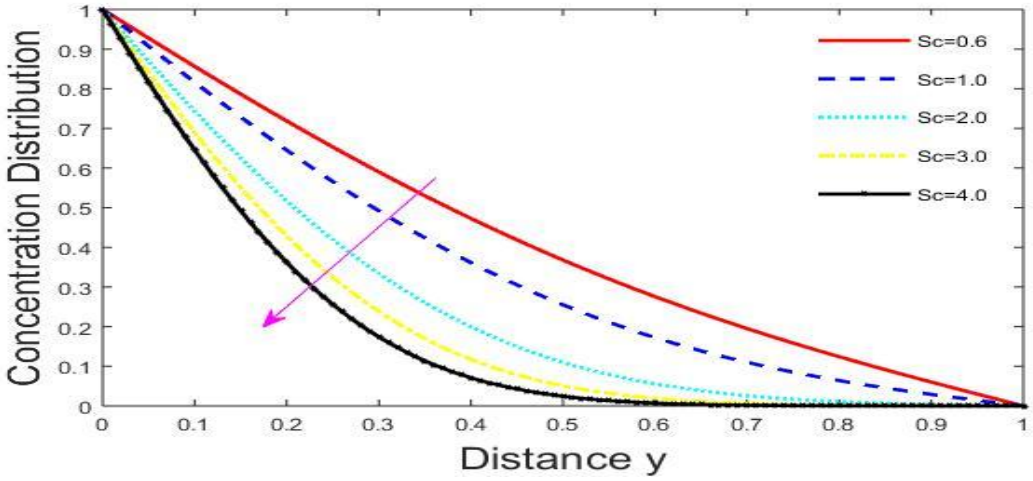

Figure 16: Effect of Schmidt parameter (Sc) on Concentration Profile

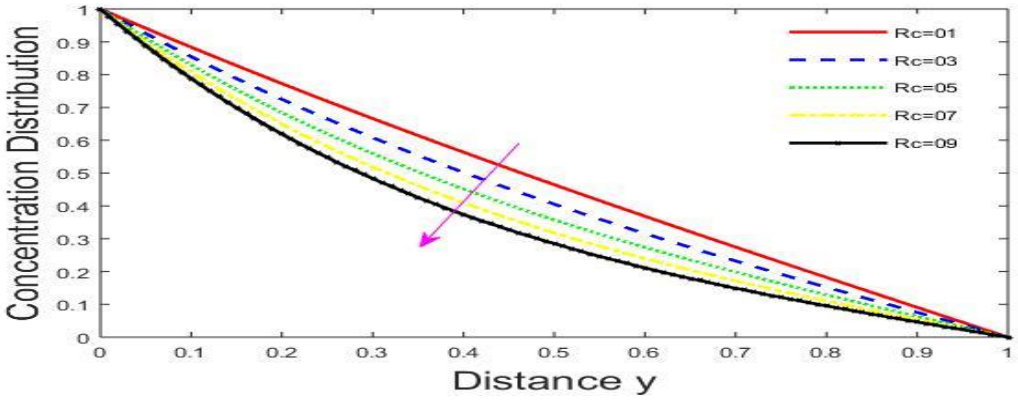

Figure 17: Effect of Chemical Reaction parameter (R_c) on Concentration Profile

Figures 16 and 17 show the effects of mass transfer parameters on concentration. Increasing the Schmidt number Sc (Figure 16) reduces the concentration distribution because larger Schmidt numbers correspond to lower mass diffusivity. Likewise, increasing the chemical reaction parameter Rc (Figure 17) decreases concentration due to the accelerated consumption of the diffusing species, resulting in a thinner concentration boundary layer.

7 Conclusion

This study investigated the combined effects of magnetohydrodynamics (MHD), porous medium resistance, viscous dissipation, thermal radiation, and chemical reaction on heat and mass transfer in a Casson fluid within a microchannel. The governing equations were solved numerically using an implicit finite difference scheme and validated with analytical solutions obtained through the perturbation technique. Excellent agreement between the two methods confirmed the accuracy of the numerical approach.

The results showed that thermal and solutal buoyancy forces enhance fluid velocity, while the Casson parameter, magnetic parameter, and porous medium resistance suppress the flow. Increasing the Prandtl number reduces the thermal boundary layer thickness and enhances heat transfer, whereas viscous dissipation and thermal radiation increase the fluid temperature. The concentration profile decreases with increasing Schmidt number and chemical reaction parameter due to reduced mass diffusivity and increased species consumption. Furthermore, skin friction increases with buoyancy effects, the Nusselt number increases with Prandtl number but decreases with radiation, and the Sherwood number increases with Schmidt number and chemical reaction.

These findings provide useful insight into the transport behaviour of electrically conducting non-Newtonian fluids and may be applied in thermal management systems, chemical processing, biomedical devices, and energy-related technologies.

Declaration of Conflicting Interests

The authors declare no potential conflicts of interest with respect to the research, authorship and publication of this article.

Acknowledgement

This research was funded by TETFUND under the Institution Based Research (IBR) Annual Intervention, we therefore acknowledge their immense support. Also, we appreciate Federal College of Education, Gidan Madi, Sokoto for their infrastructure support.

References

[1] Z. O. I. K. D. B. a. K. S. N. L. A. Lund, "Dual similarity solutions of MHD stagnation point flow of casson fluid with thermal radiation and viscous dissipation," *Scientific Reports,* Vols. 10, 15405, 2020.

[2] P. K. a. W. W. T. Anwar, "Unsteady MHD natural convection Casson fluid flow with thermal radiation and heat injection/suction," *Scientific Reports,* Vols. 11, 4275, 2021.

[3] H. U. K. M. &. A. M. Rasheed, "Unsteady MHD flow of casson fluid over a vertical plate with thermal radiation and chemical reaction," *Advances in Mechanical Engineering,* vol. 14(3), pp. 1-12, 2022.

[4] A. H. H. e. al., "MHD radiative Casson fluid flow with viscous dissipation and chemical reaction," *Frontiers in Physics,* Vols. 10, 920372, 2022.

[5] A. J. C. a. A. M. Rashad, "Heat transfer in porous media under KHD and radiation effects," *Journal of the Egyptian Mathematics Society,* vol. 29, 2021.

[6] M. &. Y. A. M. Abdullahi, "Magnetohydrodynamic free convection flow in a drag force with heat and mass transfer," *Journal of Applied Fluid Mechanics,* vol. 14(3), pp. 765-780, 2021a.

[7] M. &. Y. A. M. Abdullahi, "Analytical solution of MHD natural convection flow using perturbation technique," *International Journal of Applied Mathematics,* vol. 36(2), pp. 145-160, 2021b.

[8] N. A. U. I. &. K. M. Shah, "Unsteady Casson fluid with chemical reaction," *Applied Mathematics Letters,* Vols. 135, 108394, 2023.

[9] R. N. J. a. O. D. M. S. Das, "Chemical reaction effects on MHD boundary layer flow in porous medium," *Alexandria Engineering Journal,* vol. 55, pp. 293-302, 2020.

[10] W. A. K. a. A. M. M. A. Mabood, "Viscous dissipation and thermal radiation effects on MHD flow," *Journal of Molecular Liquids,* vol. 317, 2020.

[11] R. S. a. P. K. M. Ali, "Chemical reaction and mass transfer in MHD boundary layer flow," *Alexandria Engineering Journal,* vol. 61, 2022.

[12] S. Rosseland, "Astrophysik: Auf atomtheoretischer Grundlage. Berlin, Germany: Springer," 1931.

[13] T. W. H. &. K. M. I. Hayat, "Radiation and viscous dissipation effects in MHD flow of non-Newtonian fluids," *Results in Physics,* vol. 103845, p. 21, 2021.

[14] M. G. &. K. R. N. Reddy, "MHD Casson fluid flow with viscous dissipation," *Journal of Thermal Analysis and Calorimetry,* vol. 147(3), pp. 2345-2356, 2022.

[15] F. K. W. A. &. I. A. I. M. Mahood, "Radiation effects on MHD flow in drag force," *International Journal of Heat and Mass Transfer,* Vols. 148, 119083, 2020.

[16] W. &. N. M. Ibrahim, "Thermal radiation and viscous dissipation effects on MHD flow in porous media," *Heat Transfer Research,* vol. 52(6), pp. 45-60, 2021.

[17] F. G. B. J. &. R. G. K. Ali, "Effects of chemical reaction on MHD boundary layer flow and heat transfer," *Journal of Thermal Analysis and Calorimetry,* vol. 147(5), pp. 3257-3268, 2022.

[18] M. &. Y. A. M. Abdullahi, "Combined effects of thermal radiation and viscous dissipation in MHD flow," *Journal of Thermal Science and Engineering Application,* Vols. 16(4), 041015, 2024.

[19] M. I. S. &. B. T. Abdullahi, "Radiative heat transfer in non-Newtonian fluids with viscous dissipation," *Case Studies in Thermal Engineering,* Vols. 35, 102085, 2022.

[20] E. A. W. H. &. H. T. Algehyne, "MHD Casson fluid flow in a drag force with radiation and chemical reaction," *Applied Mathematics and Computation,* vol. 127567, p. 438, 2023.

[21] E. A. W. H. &. H. T. Algehyne, "MHD Casson fluid flow with radiation and chemical reaction in a porous medium," *Applied Mathematics and Computation,* vol. 127567, p. 438, 2023.

[22] O. D. M. a. A. Aziz, "Boundary layer flow of a nanofluid past a stretching sheet with a convective boundary condition," *International Journal of Thermal Sciences,* Vols. 50, no 12, pp. 1326-2332, 2011.

[23] A. J. Chamkha, "MHD flow in a porous medium," *International Journal of Engineering Science,* Vols. 34, no. 10, pp. 1177-1192, 1996.

[24] F. G. B. J. &. R. G. K. Ali, "Chemical reaction and heat transfer effects on MHD boundary layer flow," *Alexandria Engineering Journal,* vol. 61(5), pp. 3891-3902, 2022.

[25] M. F. M. S. Modest, "Radiative heat transfer," *Oxford, UK: Cathleen Sether,* no. 3rd edition, 2013.